Optimized CNN-based denoising strategy for enhancing longitudinal monitoring of heart failure

Salman Almuhammad Alali, Amar Kachenoura, Laurent Albera, Alfredo I. Hernández, Cindy Michel, Lotfi Senhadji, Ahmad Karfoul

Highlights

Optimized CNN-based denoising strategy for enhancing longitudinal monitoring of heart failure

Salman Almuhammad Alali,Amar Kachenoura,Laurent Albera,Alfredo I. Hernandez,Cindy Michel,Lotfi Senhadji,Ahmad Karfoul

- Reliable long-term remote heart monitoring based on an optimized denoising and classification pipeline.
- Pretrained CNN kernels as a powerful tool for denoising heart vibration signals of cardiac implant in the gastric fundus.
- Machine Learning classifier as a mean to evaluate the segmentation accuracy in the absence of a ground truth.

Optimized CNN-based denoising strategy for enhancing longitudinal monitoring of heart failure

Salman Almuhammad Alali[a], Amar Kachenoura[a], Laurent Albera[a], Alfredo I. Hernandez[a], Cindy Michel[b], Lotfi Senhadji[a] and Ahmad Karfoul[a,*]

[a]Univ. Rennes, Inserm, LTSI - UMR 1099, Campus de Beaulieu, Rennes, F-35000, France
[b]CardiaMetrics, La Tronche, Auvergne-Rhône-Alpes, Grenoble, 38700, France

ARTICLE INFO

Keywords:
Heart failure
Gastric implant
Denoising
Cardiac vibration
Cardiac event segmentation
Matrix/tensor factorization
CNN
Classification.

ABSTRACT

Cardiac vibration signal analysis emerges as a remarkable tool for the diagnosis of heart conditions. Our recent study shows the feasibility of the longitudinal monitoring of chronic heart diseases, particularly heart failure, using gastric fundus implants. However, cardiac vibration data, captured from the implant, positioned at the gastric fundus, can be highly affected by different noises and artefacts. This study introduces a novel methodology for addressing denoising challenges in the longitudinal monitoring of chronic heart diseases, using gastric fundus implants. More precisely, a novel method is designed, by repurposing pre-trained convolutional neural network models, originally designed for classification tasks, with adequately chosen convolution filters. The proposed approach efficiently tackles noise and artefacts reduction in the acquired accelerometer signals. Moreover, the integration of additional Hilbert and Homomorphic envelopes enhances the implant's ability to better segment heart sounds, namely S1 and S2. The quality assessment of this denoising strategy is performed, in the lack of ground truth, by rather evaluating its impact on a classification stage that is introduced to the proposed pipeline. Compared to standard denoising matrix factorization and tensor decomposition-based methods, results on a real 3D accelerometer dataset acquired from a set of pigs, with and without heart failure, demonstrate the efficacy of such a proposed optimized CNN-based approach with the best balance between enhancing the segmentation accuracy and preserving a maximum usable record.

1. Introduction

Heart Failure (HF) stands as a perilous global health concern, exacerbated by the aging population and impacting approximately 15 million individuals in Europe, with a notable medium-term mortality rate [1, 2]. The occurrence of Severe Heart Failure Decompensation (SHFD) frequently results in recurrent hospitalizations, presenting significant health and economic challenges [3]. Consequently, various national health systems are actively working to alleviate the burden of repetitive hospitalizations associated with HF [4, 5]. In addressing this issue, early identification of SHFD proves crucial [5, 6]. A comprehensive understanding of heart function and its conditions combined with long-term monitoring and diagnosis of these functions are paramount for reliable early detection of SHFD [7].

Heart functions encompass two primary mechanisms: mechanical and electrical which can be captured, respectively, using ElectroCardioGram (ECG) and PhonoCardioGram (PCG) recordings [8] (an example of these recordings is provided in Figure 1. The mechanical facet involves the systolic contraction and diastolic relaxation, generating two main components, S1 and S2, which respectively correspond to the first and the second heart sound in the PCG signal [9, 10]. Regarding the electrical mechanism, it coordinates the timing of muscle contractions [10]. These two mechanisms are highly disrupted in the case of HF, where a modification in muscle contractions and alterations in heart sound patterns are to be noticed. Detecting these alterations is crucial for timely intervention and effective management of heart conditions [11]. Traditionally, ECGs and PCGs signals are recorded in a non-invasive manner via chest-placed sensors [12]. While these methods are effective for short-term monitoring and diagnosis, their non-invasive acquisition manner has limitations in continuous, long-term monitoring due to the need for external equipment and patient compliance.

Alternatively, Implantable Cardiac Electronic Devices (ICEDs) are increasingly acknowledged as reliable solutions for the longitudinal monitoring of heart conditions [13]. These devices incorporate micro-implantable accelerometer sensors, which provide the advantage of indirectly capturing heart sounds, specifically, S1 and S2 waves which offer a valuable visualization of the mechanical activity of the heart, as discussed in previous studies [14, 15, 16, 17, 18, 19]. Indeed, capturing S1 and S2 heart sounds is essential for assessing heart valve functionality and mechanical performance, vital for diagnosing conditions resulting from mechanical cardiac dysfunctions, such as HF, which might be undetectable through ECG monitoring. In this context, several studies in our research group have confirmed the ability to characterize heart functions using cardiac vibration signals that are captured using 3D ACCelerometer (ACC) sensors [20, 21, 22, 17, 18, 19]. The relevance of recent work in monitoring heart functions through the processing and segmentation of cardiac vibrations using heart vibration

*This work was supported in part by the ANR-DiGS project 18-CE19-0008-03 and in part by Brittany Region DeMuG project 2497 .
*Corresponding author
ahmad.karfoul@univ-rennes.fr (A. Karfoul)
ORCID(s): 0000-0002-3977-9141 (A. Karfoul)

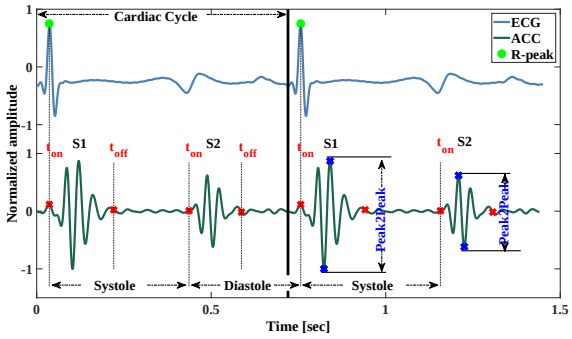

Figure 1: Synchronized Electrocardiogram (ECG) and ACCeleration (ACC) signals highlighting the R-peak, systole, and diastole periods and also the peak-to-peak amplitudes of S1 and S2 sounds.

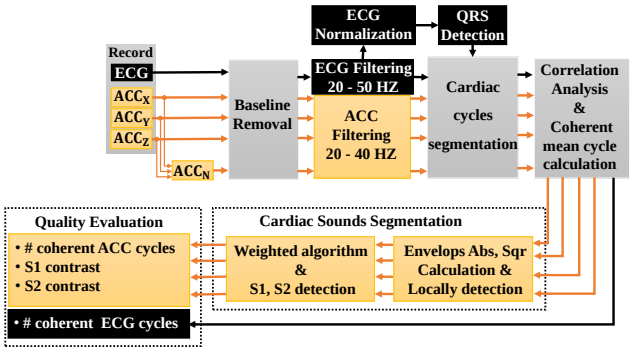

Figure 2: Data Processing Chain Diagram - Illustrates the processing pipeline for acquired data: black for the ECG signal processing steps, light yellow for the ACC (accelerometry) signal processing steps, and gray for shared signal processing steps [19].

signals from 3D ACC sensors in a gastric fundus implant has been established [19]. However, the efficacy of this approach was impacted by the relatively elevated noise levels present at the gastric site. More specifically, only 68% of the recorded data were utilized in [19] due to the presence of high-level gastric noise. This, in turn, results in less effective monitoring of heart functions.

Therefore, our primary motivation is to improve the monitoring of heart functions by utilizing 3D ACC signals from a gastric implant. In pursuit of this goal, the contribution of the current study is enhancing the overall processing pipeline recently developed by our group and illustrated in Figure 2 by incorporating a Convolutional Neural Network (CNN)-based filtering step thereby increasing the number of accepted records. The essence of our approach lies in the CNN's capacity to extract features from the network input, particularly in the early convolution layers, which are presumed to be highly correlated with the target pattern. Furthermore, in conjunction with the CNN-based filtering, a robust heart event detection step utilizing both Hilbert (Hilb) and homomorphic (Homo) envelopes is employed. The efficacy of the proposed CNN-based approach is evaluated based on accepted recordings and the capacity of the segmented S1 and S2 waves to classify the analyzed database into normal and abnormal categories. A performance comparison study, with conventional matrix factorization techniques such as Principal Component Analysis (PCA) [23], Canonical Correlation Analysis (CCA) [24], Independent Component Analysis (ICA) [25], and the tensor Canonical Polyadic Decomposition (CPD) approach [26], is also conducted.

2. Dataset

The dataset in this study was acquired using an innovative gastric implant prototype [27] used in the previous work of our research group [19]. In a few words, this implant, depicted in Figure 3, comes in two models, V1 and V2, which were utilized to capture synchronized ECG and 3D ACC signals. Specifically, the V1 model was employed to obtain data from healthy pigs, while the V2 model was utilized to record ECG and 3D ACC signals from pigs afflicted with heart failure. It's important to note that the equipment used in both V1 and V2 implants is completely identical. The modifications made to the V2 implant were limited to improve the energy consumption and reducing the implant size (see [19] for more details). These technical refinements do not affect the signal acquisition, processing capabilities, or signal quality. Consequently, the implant version does not introduce any variability or act as a confounding factor in the analysis of ACC signals. Both V1 and V2 models provide 3D ACC signals at a consistent sampling frequency of 4 kHz. More precisely, animal data were collected from 4 healthy pigs and 3 pigs with HF over a period of 14 days using an implant positioned in the gastric fundus.

This animal dataset is significantly affected by noise and artefacts originating from various sources. For instance, one artefact is introduced from gastric site activities. The mechano-physiological actions of gastric and surrounding muscles, along with respiratory movements, affect the accelerometer. Other artefacts, such as pig growls and atypical digestive sounds and movements, may also occur during the data acquisition process. Additionally, another noise arises from the implant itself. During each hourly data collection, the implant shifts from sleep to active mode for a 30-second period, generating low-frequency noise during this transition. This noise has the potential to saturate the amplifier, rendering the initial second of each record unreliable and thus disregarded during data processing. An illustration of a heart ACC signal obtained from the thorax and another acquired from the gastric implant is presented in Figure 4 (a) and Figure 4 (b), respectively. Consequently, the presence of all these noises and artefacts makes the handling of this dataset very challenging.

3. Background

This section outlines the workflow recently proposed in our research group [19], for segmenting S1 and S2 heart

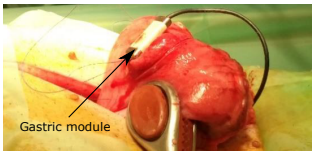

(a) Gastric module

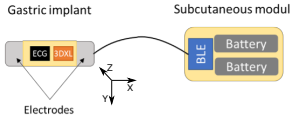

(b) Implant V1

(c) Physical design of V1

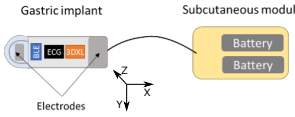

(d) Implant V2

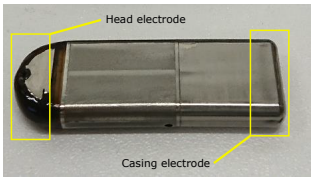

(e) Physical design of V2

Figure 3: Implant prototypes used for acquiring the ECG and ACC data, (a) A module at the pig gastric site (b) Schematic representation of the implant V1, (c) Physical design of implant V1, (d) Schematic representation of implant V2, (e) The physical design of the gastric module of the implant V2 [19]. ECG: ElectroCardioGram module. 3DXL: 3D Accelerometer module. BLE: Bluetooth module.

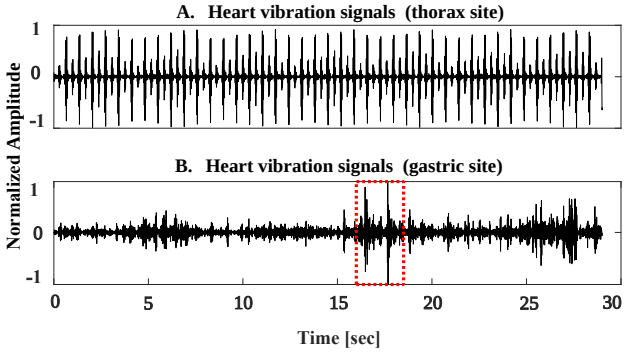

Figure 4: Heart vibration signals: a) Clean cardiac vibrations acquired from the thorax, and b) Noisy cardiac vibration signals acquired from the gastric fundus. The red rectangle highlights odd peaks, potentially caused by pig growls or gastrointestinal movements

sounds. As depicted in Figure 2, this detection approach relies on using the acquired synchronized ECG and ACC signals of the seven pigs. More precisely, for each record being introduced to the above-mentioned workflow, the following steps are applied. (i) **Baseline removing** is firstly applied to ECG, the 3D ACC signals (i.e., ACC_x, ACC_y, ACC_z) and the associated ACC norm signal denoted by $ACC_N = \sqrt{ACC_x^2 + ACC_y^2 + ACC_z^2}$. Typically, a robust locally weighted linear regression technique is applied on ECG and each ACC component for baseline removal [28]. (ii) **Band-passe filtering** is then performed on ECG signals in the frequency band $[20 - 50$ Hz$]$ to highlight the R-peak followed by a local normalization based on minimum/maximum values as suggested in [28]. ACC signals are also filtered in the frequency band $[20 - 40$ Hz$]$, to target the maximum energy of local cardiac accelerometer signals. (iii) **Cardiac cycles segmentation** is done using the modified Pan–Tompkin QRS detector [29]. R-peaks are then identified, allowing for the mapping of ECG segmentation onto the synchronized ACC signals. It is noteworthy that as resulting cycles might have different lengths, their respective durations were aligned to the median lengths for consistency. (iv) **Correlation and coherence analysis** of the segmented ACC was conducted. Then a coherent mean cycle is computed for each ACC axis as the average of those ACC cycles whose correlation coefficient exceeds 0.6. (v) **Cardiac sound segmentation** step segments the coherent mean cycle into the S1 and S2 heart sounds by utilizing an algorithm that analyzes both absolute and squared envelopes [21]; then a dynamic threshold is applied to identify local instants of heart sounds across each ACC axis. Subsequently, a fusion-weighted algorithm integrates these detection instants [19], identifying the final onset and offset times of S1 and S2.

Finally, the quality of the recordings was evaluated after applying the processing steps described earlier. This post-processing step aims to select only the recordings with an acceptable SNR that permits a robust segmentation of S1 and S2 [19]. In more detail, this post-processing process focuses on two main acceptance criteria: **a)** the percentage of coherent ECG and ACC cycles, and **b)** the contrast between S1 and S2 relative to the background noise. Specifically, the contrast of an event is defined as the ratio of the standard deviation of the useful signal (S1/S2) to the background noise, which includes the interval from the end of S1 to the start of S2. An event contrast ratio of 2 or more is deemed significant, indicating that S1 and S2 are distinctly discernible against the background. Therefore, a recording is considered acceptable if it contains at least three coherent ECG cycles and two ACC cycles, and if the contrast of S1 and S2 with respect to the background noise is equal to or greater than two. Recordings that do not satisfy these criteria are rejected. Hence, after this quality assessment process, only about 68% of the data collected over a 14-day period was retained. This is essentially due to the high noise levels at the collection site, which is not conducive to accurate detection of the exact moments marking the start and end of heart events.

4. Methodology

To tackle the noise challenge in the intricate dataset under consideration, the original homemade workflow [19], as illustrated in Figure 2, was revisited in this study. This reassessment aims to ensure a more reliable cardiac cycle segmentation and effective denoising of heart sounds. An overview of the modified workflow is depicted in Figure 5. The main contributions of this study are the following:

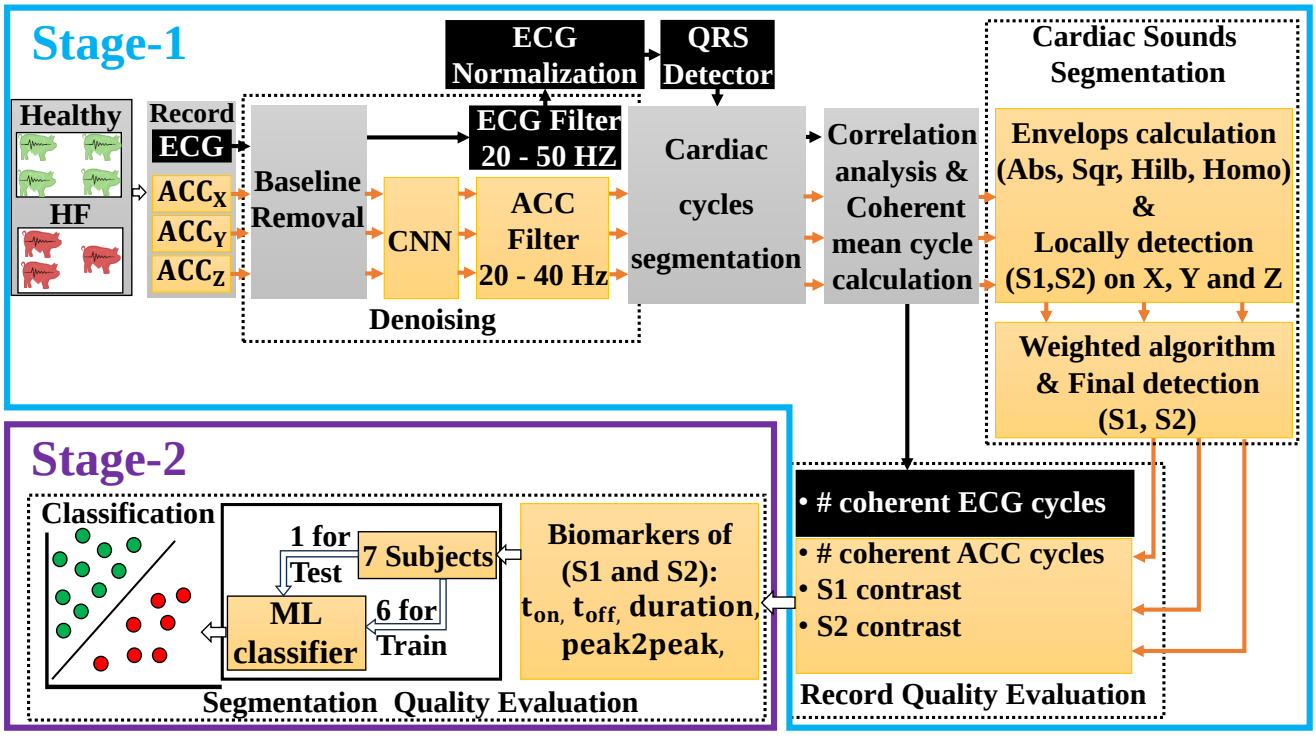

Figure 5: The comprehensive diagram illustrates the full pipeline applied to the dataset. Black boxes denote the ECG signal pipeline, while light yellow boxes represent the ACC signals pipeline, and gray boxes indicate processing steps shared between the ECG and ACC signals

- Increasing the number of accepted records by incorporating a CNN-based denoising step into the original workflow as illustrated in Figure 5. Specifically, a pre-trained low-cost CNN model initially developed for classification tasks is repurposed for denoising ACC signals with kernels being adequately chosen.
- Enhancing the cardiac sound segmentation by considering additional envelopes, such as Hilb and Homo.
- Introducing a machine learning-based classification module for evaluating the quality of cardiac sound segmentation.

A more detailed description of these contributions will be provided in the subsequent sections.

4.1. Standard denoising methods

Traditional denoising techniques that have been investigated in the current study are categorized into a) **Matrix factorization-based methods** such as Principal Component Analysis (PCA) [30], Canonical Correlation Analysis (CCA) [24] and the widely recognized Independent Component Analysis (ICA) method known as Efficient FastICA (EFICA) [31]. All the above-mentioned methods were applied to a matrix of ACC signals with dimensions specified as (number of axes × number of time samples), where the number of axes is three (i.e., ACC_x, ACC_y, ACC_z) and the length of the signal is 116000 samples (corresponding to 29 sec with a sampling frequency of 4KHz). b) **Tensor decomposition-based methods** such as Canonical Polyadic Decomposition (CPD) [26, 32]. As tensor-based methods necessitate a multidimensional representation of the data, a three-order data tensor of size (Number of axes × Cycle duration × Number of cycles) is constructed in the current study. This is achieved by initially creating a set of space-time matrices, each of size (Number of axes × Cycle duration), where each matrix captures a segmented cycle over the three ACC axes. Subsequently, these space-time matrices are stacked sequentially to form the data tensor.

4.2. Deep learning-based denoising

CNN models are recognized for their capability to filter out noise and extract valuable features from data through different filters, known as kernels [33, 34]. This enables CNNs to capture both the context and the patterns present in both the signal and the noise [35]. Our objective is to identify the most effective kernel in a CNN model for achieving the highest noise rejection ratio at the level of the feature map. As the noise level directly affects the classification quality of healthy and HF pigs in our context, our approach relies on resorting to a pre-trained low-cost but efficient CNN model designed for such classification tasks. Subsequently, a block of very few convolution layers with the best filter is used to denoise the ACC signals. Details on the pre-trained CNN model and the choice of the best kernel are extensively discussed hereafter.

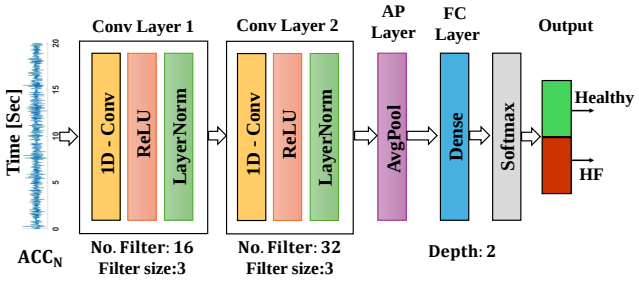

Figure 6: Architecture of the proposed convolutional neural network (CNN).

4.2.1. CNN training for classification

In order to train the network for the classification task, a 1D-CNN model was constructed. Figure 6 shows that the proposed network comprises two one-dimensional convolutional layers. The first layer consists of 16 convolutional filters (i.e., kernels) each with a length of 3, followed by a ReLU activation function and a layer normalization. Subsequently, the second layer consists of 32 filters also with a length of 3, followed by the ReLU activation function and a layer normalization. Afterward, an Average Pooling (AP) layer, a Fully Connected (FC) layer, a softmax layer, and finally, an output layer, are used.

To train the CNN model, the dataset described in section 2 is used. The norm axis signal ACC_N is the only time series being introduced to the input of the 1-D CNN to differentiate between healthy and HF pigs. All ACC_N signals underwent simple pre-processing steps before being introduced to the network. These pre-processing steps include centering and baseline removal as suggested in [28].

Recall that the dataset comprises signals acquired from 7 pigs (3 healthy and 4 with HF). According to Table 1, the data set, consisting of 999 records, exhibits a significant variation in the number of records among the pigs. For instance, the 7th pig has only 50 records, whereas the 4th one has substantially a higher number of records (i.e., 316 records). To ensure reliable training of the neural networks especially in the case of limited datasets, the data augmentation technique is used in this study as its relevance has been confirmed in various CNNs. The data augmentation process applied to the dataset involves overlapped segmentation, a common technique in biosignal processing. Specifically, from each 29-second recording, we use a 20-second sliding window to extract multiple segments. Each new 20-second segment is obtained by shifting the sliding window forward by 1 second. This 1-second shift allows for the generation of a new segment, and the sequence is repeated until the end of each recording. As a result, 10 distinct 20-second segments are generated from each original recording, effectively increasing the size of the dataset by a factor of 10.

To guarantee a training process that is not only effective and reliable but also generalizable, a Leave-One-Out (LOO) pig cross-validation approach was employed. In this methodology, for each training sweep, the 1D-CNN is trained on the records of only 6 pigs out of 7 ones. Subsequently, the trained model is evaluated using the data from the remaining 7^{th} pig, which serves as the test subject. Upon completing this process for all the 7 subjects, the classification results from the seven distinct models are accumulated into one confusion matrix. This method allows for the assessment of the model overall performance and its generalization capabilities to unseen data, thereby verifying its applicability and reliability in real-world scenarios.

Obtained classification results in terms of sensitivity, specificity, F-score, and accuracy are respectively 0.9813, 0.9935, 0.9844, and 98.93%. These results suggest that the proposed 1D-CNN can capture, from very noisy ACC signals, reliable features permitting an efficient distinction between the healthy and HF classes of records. Indeed, this suggests that the ACC data hold valuable information for diagnosing heart conditions, particularly in the context of HF.

4.2.2. Pre-trained CNN as a denoising filter

It's known that in sophisticated CNN-based models with deep architectures, the filters in the early layers of the network tend to detect simple patterns, whereas those in deeper layers identify more complex and comprehensive ones. This hierarchical learning approach enables CNNs to understand data at multiple levels [36, 35]. In this study, as mentioned earlier, the objective is to utilize the CNN model as a denoising filter while retaining most of the information related to S1 and S2 waves. Consequently, a low-cost 1D-CNN model, consisting of only two convolutional layers as depicted in Figure 6, is employed. Using the pre-trained 1D-CNN as a denoising filter entails selecting the optimal kernels for both convolution layers. To this end, a greedy search strategy to evaluate the filters associated with the two convolution layers of the pre-trained 1D-CNN is adopted. The best-learned filter in the CNN model is determined based on its ability to effectively reject noise while preserving the shape of the S1 and S2 waves thereby providing the highest acceptation ratio of the ACC records (i.e., the filter that permits the most accurate segmentation of S1 and S2). The retained best-learned filters together with the two convolution layers can be integrated to form a CNN-based denoising block that is applied after a baseline removal pre-processing step as shown in Figure 7. It is worth mentioning that the same greedy search strategy is also applied to select the best component (or set of components) when the PCA, CCA, EFICA, and CPD methods are applied.

4.3. Envelopes

As stated in Section 3, the segmentation of cardiac cycles into the primary heart waves, S1 and S2, follows the methodology outlined in [21]. This method relies on computing both the absolute (Abs) and squared (Sqr) envelopes. Additionally, alongside the Abs and Sqr envelopes, which are calculated entirely in the time domain, the Hilb and Homo envelopes, derived in the frequency domain, are also utilized. This approach is illustrated in Figure 8 (a). Despite being calculated in the frequency domain, these

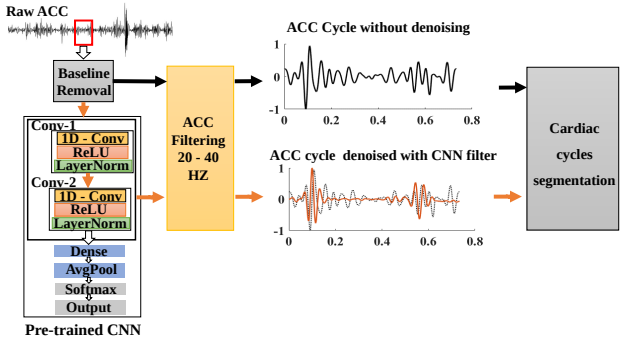

Figure 7: An example of processing an ACC signal, focusing on a single ACC cardiac cycle presented in two distinct methods: 1) without denoising, shown in black; and 2) with denoising, using pre-trained convolutional filters, displayed in orange.

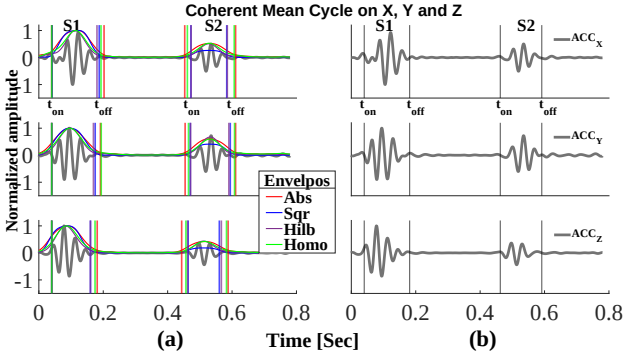

Figure 8: (a) The coherent mean cycles over the three ACC axes (X, Y and Z) showcasing the Absolute (Abs), Squared (Sqr), Hilbert (Hilb) and Homomorphic (Homo) envelopes along with their corresponding four detected time instants for both S1 and S2 waves ($t_{S1_{on}}$, $t_{S1_{off}}$, $t_{S2_{on}}$ and $t_{S2_{off}}$). (b) the final instants for the heart event, as detected by the detection weighted algorithm [21, 19].

additional envelopes yield meaningful results in the time domain. Note that, the Hilb envelope is obtained from the Hilbert transform of the ACC signal [37], while the Homo envelope is generated by low-pass filtering the natural logarithm of the analytic ACC signal computed using the Hilbert transform [38, 9]. Figure 8 (a) shows the four envelopes – Abs, Sqr, Hilb, and Homo – calculated for the coherent mean ACC cycles across the X, Y, and Z axes. Each of these four envelopes provides, for each event over the three denoised ACC axes, four possible detection instants. Consequently, this yields a total of 12 detections for each individual instant associated with the heart events. The final instants for each point $t_{S1_{on}}, t_{S1_{off}}, t_{S2_{on}}$ and $t_{S2_{off}}$, shown in Figure 8 (b), are determined using the fusion-weighted algorithm [21, 19]. This strategy enhances the robustness of the heart sound segmentation for S1 and S2, thereby enabling the preservation of larger recordings (see 6 for more details).

5. Evaluation criteria

Evaluating the quality of S1 and S2 segmentation on the dataset at hand is challenging due to the absence of ground truth annotations for heart events. This makes a conventional evaluation of our segmentation pipeline impractical. Several studies [39, 40, 41] clearly demonstrate that enhancing segmentation quality through appropriate preprocessing generally improves classification performance. In other words, effective denoising directly influences segmentation quality, which in turn affects classification accuracy. Building on this concept, we propose to evaluate the segmentation quality of S1 and S2 waves using a criterion based on classification metrics (healthy vs. HF). In this manner, the classification task serves as a hint of ground truth, as the most accurate classification (in terms of Sensitivity, Specificity, Precision, F-Score, and Accuracy) of heart records corresponds, as we expect, to the most precise segmentation quality. In turn, the most precise segmentation quality indicates the most effective denoising approach. This relationship underscores the importance of robust segmentation techniques in enhancing the overall performance of classification algorithms for heart-related data.

As the characteristics of heart mechanical events, specifically S1 and S2, are essential for detecting cardiac abnormalities [42, 43], features associated with these events are mainly used to differentiate between healthy and pathological records. The selected features include the onset and offset instants, durations, peak-to-peak amplitudes of S1 and S2 heart events, and the ratio between peak-to-peak of S1/S2. These features are clinically significant in diagnosing heart failure, as addressed by several studies [42, 44, 45]. The available class labels with the set of the aforementioned features are then introduced to learn a simple classifier as extensively described in Section 6. This classification task will be conducted exclusively on records that meet the acceptance criteria as outlined in [19]. More specifically, records must exhibit at least 2 coherent cycles in the ACC data and a contrast of S1 and S2 with respect to the background that exceeds 2 in the cardiac cycle.

6. Results

This section presents the main findings of the current study. Initially, it explores the impact of the proposed 1D-CNN denoising technique on the acceptance rate of cardiac records obtained from the gastric implant. This impact is quantified using a hint of ground truth that is made possible thanks to a classification step of healthy vs. HF records. It's important to recall that only the records deemed acceptable following the denoising step are considered for segmenting both S1 and S2 waves. Subsequently, their various associated features, as described earlier for classification purposes, are computed as illustrated in the proposed pipeline depicted in Figure 5.

As far as the classifier is concerned, various algorithms are examined, including Logistic Regression (LR), Support Vector Machine (SVM), Random Forest (RF), K-Nearest

Table 1
Distribution of accepted records per pig for each denoising method

Class	Pig	Total number of records	Number of accepted records **Denoising method**					
	ID	-	Ed-Ref [19]	PCA	CCA	EFICA	CPD	**CNN**
Healthy	1	95	81	80	75	72	82	**87**
	2	163	132	132	124	137	132	**144**
	3	232	189	196	196	190	188	**217**
	4	316	288	284	265	275	286	**311**
HF	5	70	57	54	55	57	59	**46**
	6	73	66	61	64	63	67	**53**
	7	50	46	43	40	34	46	**48**
	All	999	859	850	819	828	860	**906**
	-	-	85.98%	85.08%	81.98%	82.88%	86.09%	**90.69%**

Neighbors (KNN), Adaptive Boosting (AdaBoost), and Naive Bayes (NB). Each algorithm was tested with multiple configurations to determine the most effective one for the classification task. Following the conducted tests, the Naive Bayes (NB) classifier with a triangular kernel is selected for integration into our pipeline evaluation, as it exhibited the highest classification performance and produced the best overall results. A comparative study with the original pipeline (without additional denoising block) and four traditional denoising techniques, namely PCA, CCA, EFICA and CPD, is also provided.

6.1. Impact of denoising and used envelopes on data quality

The data quality stands as an important aspect of the current study since it shows the efficiency of the longitudinal monitoring process in producing valuable records that can reflect the actual heart conditions. Table 1 shows the distribution of accepted records both for individual pigs and the entire dataset. This table shows a biased distribution, with 806 records acquired from four healthy pigs and only 193 HF records from three pathological pigs. The initial pipeline shown in Figure 2 utilized this dataset by accepting 553 healthy and 127 HF records, representing 68.07% of the total dataset [19]. Records failing to meet the established quality criteria, such as the number of coherent cycles and contrast heart events (S1/S2) compared to the background noise, were rejected from the dataset.

First, the current study investigates the impact of incorporating Hilb and Homo envelopes, as detailed in Section 4, on the percentage of accepted records. This step was taken before implementing any further modifications to the initial pipeline depicted in Figure 2. The initial pipeline, with Hilb and Homo envelops being incorporated into the segmentation of S1 and S2, is referred to in the sequel as the *edited reference pipeline* (in short, Ed-Ref [19]). The Ed-Ref pipeline shows a record acceptance rate of 85.98% (see Table 1). This rate comprised 690 records from healthy subjects and 169 records from subjects with HF. In fact, the use of the four envelopes (Abs, Sqr, Hilb, and Homo) rather than the two ones (Abs and Sqr), resulted in exploiting the dataset more effectively, leading to about an 18% increase in the number of accepted records compared to the reference pipeline [19]. Consequently, all subsequent analyses and evaluations of the considered denoising methods will be conducted on the ED-Ref pipeline.

Regarding the denoising step in the proposed pipeline depicted in Figure 5, various denoising strategies were explored, such as matrix factorization and tensor decomposition, each yielding different numbers of accepted records, as illustrated in Table 1. The employment of matrix factorization techniques resulted in the following record acceptance rates: PCA yielded 85.08% (692 healthy and 158 HF), CCA [24] led to 81.98% (660 healthy and 159 HF), and EFICA [31] achieved 82.88% (674 healthy and 154 HF). For the tensor decomposition-based denoising strategy, CPD achieved a record acceptance rate of 86.09% (688 healthy and 172 HF records). Now, with the pre-trained CNN, including wisely selected filters, being used as a denoising tool, a record acceptance rate of 90.69% (759 healthy and 147 HF) was obtained. Compared to the reference pipeline shown in Figure 2, the incorporated denoising step together with the additional envelops (Hilb and Homo) for S1 and S2 segmentation enhanced the records usability by approximately 12% to 22% over the same monitoring period, thereby providing more comprehensive insights into heart conditions. The pre-trained CNN with those associated learned filters, that are adequately selected, outperforms all the other classical denoising strategies in terms of the record acceptance ratio.

6.2. Impact of denoising on the quality of S1 and S2 segmentation

In the subsequent stage of the conducted study, we focused on selecting features associated with the primary cardiac events, S1 and S2, for classifying the records as either healthy or pathological. The selected features include the onset and offset instants, durations, peak-to-peak amplitudes of the first (S1) and second (S2) heart events, and the ratio between peak-to-peak of S1/S2 events as shown in Figure 1. These features are clinically significant in diagnosing of HF, as pointed out by several studies [42, 44, 45]. The seven extracted features from each record are then assembled into a seven-dimensional feature vector. This process generates a dataset with N records per scenario, as shown in Table 1, where each record is represented by a seven-dimensional feature vector usedfor training or testing the classifier. In this study, two classical classification strategies

are employed to evaluate the performance of the proposed pipeline. The first strategy uses bootstrapping to assess the model's performance stability and reliability by repeatedly sampling the dataset with replacement. The second strategy, Leave-One-Subject-Out (LOO), is adopted to evaluate the generalizability of the proposed methodology, providing a stringent assessment of the model's performance on entirely new subjects.

6.2.1. Bootstrap classification strategy

Given the imbalance issue in our database, with healthy records four times outnumbering pathological ones, it was necessary to balance the dataset for unbiased classification performance. To this end, all HF records were included but only a number of HF records that is equal to the number of healthy ones were randomly selected. Next, the dataset was split into 90% as a training set and 10% as a testing set. This process of random selection of HF records and data splitting was performed over 100 independent trials. Finally, the average classification performance across these trials was computed. Recall that, the classification task was designed to distinguish between healthy and HF cardiac records, based on automatically extracted clinical features of segmented S1 and S2 heart sounds using the proposed pipeline shown in Figure 5. Obtained results are illustrated in Table 2. According to this table, the pipeline Ed-Ref [19], without any denoising step, achieved a Sensitivity of 0.772, a Specificity of 0.830, a Precision of 0.809, an F-Score of 0.763 and an overall Accuracy of 0.776. The use of matrix factorization-based methods (PCA, CCA, and EFICA) marginally enhanced the classification quality, whereas the CPD approach slightly deteriorated the classification performance. Regarding the proposed 1D-CNN denoising approach, it significantly improved the results, achieving a Sensitivity of 0.879, a Specificity of 0.938, a Precision of 0.935, an F-Score of 0.906 and an overall Accuracy of 0.909.

6.2.2. Leave-One-Subject-Out classification strategy

Besides, a non-pig specific strategy was also investigated to ensure a more reliable and realistic assessment of the proposed methodology. More precisely, given the limited number of subjects in our dataset (7 pigs), we adopted a Leave-One-Out (LOO) procedure. This involved training the ML classifier using data from 6 pigs and testing it on the left-out, unseen 7th pig. This ensures that the classifier was trained on both classes before being tested. More precisely, testing the Pig_{α}, $\alpha = 1:7$, consists of classifying each of its records as Healthy or HF. This process was repeated seven times, with each pig serving as a test subject once. Importantly, we did not calculate performance metrics separately for each individual test. Instead, after completing all seven testing processes, we accumulated the results into a single confusion matrix, and then the classification criteria were calculated. As expected, the outcomes of this LOO pig classification, as detailed in Table 3, show clearly that in all cases the obtained performance is lower than that presented in Table 2, especially in terms of Sensitivity, Precision, and F-Score. Nevertheless, the obtained results clearly exhibit that the proposed 1D-CNN based denoising method is still very effective, even when a non-pig specific strategy is adopted. Indeed, the use of filters learned from pre-trained 1D-CNN demonstrated the highest performance across all metrics, with a Sensitivity of 0.809, a Specificity of 0.976, a Precision of 0.868, an F-Score of 0.838 and an Accuracy of 0.949.

Table 2
Classification results with different denoising scenarios, the results with 100 times bootstrapping strategy

Method	Sensitivity	Specificity	Precision	F-Score	Accuracy
Ed-Ref [19]	0.722	0.830	0.809	0.763	0.776
PCA	0.755	0.852	0.836	0.793	0.803
CCA	0.74	0.807	0.793	0.765	0.773
EFICA	0.761	0.852	0.838	0.797	0.807
CPD	0.732	0.775	0.765	0.748	0.753
CNN	**0.879**	**0.938**	**0.935**	**0.906**	**0.909**

Table 3
Classification results with different denoising scenarios, the results with leave one pig out strategy

Method	Sensitivity	Specificity	Precision	F-Score	Accuracy
Ed-Ref [19]	0.615	0.842	0.488	0.544	0.797
PCA	0.626	0.875	0.535	0.577	0.829
CCA	0.626	0.878	0.553	0.587	0.830
EFICA	0.636	0.878	0.531	0.579	0.835
CPD	0.598	0.843	0.488	0.537	0.794
CNN	**0.809**	**0.976**	**0.868**	**0.838**	**0.949**

7. Discussion

Implantable gastric devices offer many advantages, including continuous monitoring of chronic heart conditions such as heart failure and the ability to effectively pick up changes in heart rhythm, enabling timely intervention and appropriate treatment adjustments. However, the main challenge for continuous heart condition monitoring using such implants is challenging due to the inevitable multi-source artefacts related to the gastric acquisition site, which primarily affects the crucial ACC signals in extracting cardiac events (S1 and S2), as stated by a previous work of our research group [19]. In fact, two primary limitations are identified in the data at hand: (i) the presence of noise and artifacts in the ACC signals, hindering the accuracy of S1 and S2 wave segmentation, and (ii) the relatively limited amount of accepted records overall the dataset. Improving the quality of heart sound segmentation in data acquired from implantable gastric devices for reliable heart condition monitoring was hence the main concern of the current study.

This study addressed the previous work limitations by introducing two contributions to the original pipeline depicted in Figure 2: (i) the use of filters of a pre-trained CNN initially designed for a classification task as filters to remove noise from ACC signals, and (ii) the integration of additional envelopes (Hilb and Homo) in the segmentation step of S1 and S2 waves. Furthermore, due to the unavailability of ground truth annotations for heart events (S1 and S2), we

employed a strategy based on the evaluation of an ML classifier capable of distinguishing healthy from pathological records. This served as an assessment criterion for evaluating the effectiveness of various denoising methods in enhancing the segmentation quality. Our assumption relies on the fact that accurate differentiation between healthy and HF pigs corresponds to precise segmentation of S1 and S2 waves. Consequently, superior segmentation quality signifies the most effective denoising approach.

The obtained results demonstrate the superiority of the pre-trained 1D-CNN filter in terms of both the data acceptation rate (about 5% over the original pipeline without denoising shown in Figure (2) and the classification one) for all assessed statistical metrics and both considered denoising strategies (i.e., matrix factorization and tensor decomposition based approaches). More importantly, the CNN-based denoising approach is the only one that achieved significantly better classification performance specifically in terms of Accuracy and F1-Score compared to the utilization of the other denoising methods in the case of bootstrapping and LOO pig cross-validation approaches. This demonstrates the generalization ability of the proposed CNN-based pipeline. To the best of our knowledge, this work represents the first instance of leveraging pre-trained CNN filters, originally developed for a classification task, to address a completely different challenge namely, the denoising task discussed in this paper.

Even if the obtained results are very promising, some limitations of the current study should be underlined: (i) The first one is related to the selection criteria being used for the choice of the best CNN filter. More precisely, in this study, the best filter is chosen as the one that gives the best record acceptance rate but this is without taking into account the classification rate. One possible solution is to choose the "best" filter as the one that produces the best trade-off between enhancing the percentage of acceptable records and the overall classifier performance. In the case of large datasets, it is possible to learn the best filter by splitting the data into training, validation, and test sets, and then selecting the filter based on the performance computed over the validation set. Note that, selecting the appropriate filters and configuring the CNN may be context-dependent and needs to be re-evaluated when applied to different datasets or applications. This limitation also affects other classical denoising techniques. Regardless of the method being used (PCA, CCA, EFICA, and CPD), determining the most relevant component(s)/tensor rank is necessary; (ii) The second limitation pertains to the dataset itself. Upon close examination of the results presented in Table 2 and Table 3, it is apparent that the overall accuracy achieved with the LOO pig scenario surpasses that of the bootstrapping method in most cases. At first glance, this outcome may appear unusual. This can be explained by the significant bias of the dataset towards the healthy class, which accounts for a number of examples that is four times larger than those in the HF class. In this case, the F-score criterion becomes more meaningful as it provides a balanced measure of the classifier's overall performance; (iii) The third limitation to consider is that this study was not evaluated on human data. This is currently justified by the fact that testing such implantable devices directly on humans during preclinical stages is ethically impermissible. However, extending these results to human data will be part of future research efforts to advance this embedded technology toward clinical application. It is worth noting that, the choice of a pig as an animal model is motivated by several factors: pigs exhibit anatomical, physiology, metabolism, and hemodynamic and electrophysiological features comparable to those of humans. Additionally, pigs models, with various heart pathologies, are also available [46, 47, 48, 49, 50]. Thus, pig models remain highly valuable for cardiovascular research, particularly for preclinical testing and device development [50]. The findings of this study hold promise for successful outcomes in future human applications.

8. Conclusion

This study introduced a novel methodology, possibly the first of its kind, leveraging pre-trained CNN models originally designed for classification tasks to address denoising challenges in the context of longitudinal monitoring of chronic heart diseases, particularly heart failure, using an implant located in the gastric fundus. By integrating additional Hilbert and Homomorphic envelopes and repurposing pre-trained CNN filters for denoising purposes, significant enhancements were observed in the implant's ability to effectively harness data. This resulted in improved reliability in segmenting ACC signals into key cardiac events, namely S1 and S2, thereby bolstering the implant's performance in monitoring cardiac conditions over time. Given the absence of annotated data, a machine learning classifier utilizing clinically significant features, including those associated with S1 and S2 events, was employed to evaluate denoising efficacy. Results indicated that the denoising method leveraging pre-trained CNN filters yielded the most favorable balance between enhancing segmentation accuracy and preserving the maximum amount of usable data. Overall, the methodology outlined in this study has significantly enhanced the capabilities of gastric fundus implants for long-term reliable monitoring of cardiac conditions.

ETHICS STATEMENT

The animal study was reviewed and approved by Ethics committee recognized by the French Ministry of Research.

References

[1] G. Savarese, P. M. Becher, L. H. Lund, P. Seferovic, G. M. Rosano, A. J. Coats, Global burden of heart failure: a comprehensive and updated review of epidemiology, Cardiovascular research 118 (2022) 3272–3287.

[2] B. Steiner, A. Neumann, Y. Pelz, C. F. Ski, L. Hill, D. R. Thompson, D. Fitzsimons, L. J. Dixon, J. Brandts, M. Verket, et al., Challenges in heart failure care in four european countries: a comparative study, European Journal of Public Health 33 (2023) 448–454.

[3] A. M. Epstein, A. K. Jha, E. J. Orav, The relationship between hospital admission rates and rehospitalizations, New England Journal of Medicine 365 (2011) 2287–2295.

[4] I. Ardahanli, M. Celik, Serum uric acid levels among patients who died in recent year due to heart failure with reduced ejection fraction, Journal of the College of Physicians and Surgeons Pakistan 30 (2020).

[5] M. Fudim, D. Yazdi, U. Egolum, A. Haghighat, A. Kottam, A. J. Sauer, H. Shah, P. Kumar, V. Rakita, C. Centen, et al., Use of a cardiac scale to predict heart failure events: Design of scale-hf 1, Circulation: Heart Failure 16 (2023) e010012.

[6] A. S. Desai, A. Bhimaraj, R. Bharmi, R. Jermyn, K. Bhatt, D. Shavelle, M. M. Redfield, R. Hull, J. Pelzel, K. Davis, et al., Ambulatory hemodynamic monitoring reduces heart failure hospitalizations in "real-world" clinical practice, Journal of the American College of Cardiology 69 (2017) 2357–2365.

[7] G. Shafiq, S. Tatinati, W. T. Ang, K. C. Veluvolu, Automatic identification of systolic time intervals in seismocardiogram, Scientific reports 6 (2016) 37524.

[8] S. Ajitkumar Singh, S. Ashinikumar Singh, N. Dinita Devi, S. Majumder, Heart abnormality classification using pcg and ecg recordings, Computación y Sistemas 25 (2021) 381–391.

[9] D. B. Springer, L. Tarassenko, G. D. Clifford, Logistic regression-hsmm-based heart sound segmentation, IEEE transactions on biomedical engineering 63 (2015) 822–832.

[10] K. El Houari, Modeling and imaging of electrocardiographic activity, Ph.D. thesis, Université Rennes 1, 2018.

[11] R. H. Schwinger, Pathophysiology of heart failure, Cardiovascular diagnosis and therapy 11 (2021) 263.

[12] W. Phanphaisarn, A. Roeksabutr, P. Wardkein, J. Koseeyaporn, P. Yupapin, Heart detection and diagnosis based on ecg and epcg relationships, Medical Devices: Evidence and Research (2011) 133–144.

[13] N. Varma, F. Braunschweig, H. Burri, G. Hindricks, D. Linz, Y. Michowitz, R. P. Ricci, J. C. Nielsen, Remote monitoring of cardiac implantable electronic devices and disease management, Europace 25 (2023) euad233.

[14] G. Plicchi, E. Marcelli, M. Parlapiano, T. Bombardini, Pea i and pea ii based implantable haemodynamic monitor: pre clinical studies in sheep, Europace 4 (2002) 49–54.

[15] P. Bordachar, L. Labrousse, S. Ploux, J.-B. THAMBO, S. Lafitte, P. Reant, P. Jais, M. Haissaguerre, J. Clementy, P. D. SANTOS, Validation of a new noninvasive device for the monitoring of peak endocardial acceleration in pigs: implications for optimization of pacing site and configuration, Journal of cardiovascular electrophysiology 19 (2008) 725–729.

[16] P. K. Jain, A. K. Tiwari, Heart monitoring systems—a review, Computers in biology and medicine 54 (2014) 1–13.

[17] C. Gallet, V. Le Rolle, J.-L. Bonnet, C. Henry, A. Hagège, P. Mabo, G. Carrault, A. I. Hernández, Analysis of endocardial micro-accelerometry during valsalva maneuvers, in: 2016 Computing in Cardiology Conference (CinC), IEEE, 2016, pp. 21–24.

[18] M. Calvo, J.-L. Bonnet, V. Le Rolle, M. Lemonnier, S. Yasuda, W. Oosterlinck, A. Hernández, Evaluation of three-dimensional accelerometers for the study of left ventricular contractility, in: 2018 Computing in Cardiology Conference (CinC), volume 45, IEEE, 2018, pp. 1–4.

[19] H. Areiza-Laverde, C. Dopierala, L. Senhadji, F. Boucher, P. Y. Gumery, A. Hernández, Analysis of cardiac vibration signals acquired from a novel implant placed on the gastric fundus, Frontiers in Physiology 12 (2021) 748367.

[20] E. Donal, L. Giorgis, S. Cazeau, C. Leclercq, L. Senhadji, A. Amblard, G. Jauvert, M. Burban, A. Hernández, P. Mabo, Endocardial acceleration (sonr) vs. ultrasound-derived time intervals in recipients of cardiac resynchronization therapy systems, Europace 13 (2011) 402–408.

[21] L. Giorgis, P. Frogerais, A. Amblard, E. Donal, P. Mabo, L. Senhadji, A. I. Hernández, Optimal algorithm switching for the estimation of systole period from cardiac microacceleration signals (sonr), IEEE Transactions on Biomedical Engineering 59 (2012) 3009–3015.

[22] A. I. Hernández, F. Ziglio, A. Amblard, L. Senhadji, C. Leclercq, Analysis of endocardial acceleration during intraoperative optimization of cardiac resynchronization therapy, in: 2013 35th Annual International Conference of the IEEE Engineering in Medicine and Biology Society (EMBC), IEEE, 2013, pp. 7000–7003.

[23] I. T. Jolliffe, Principal component analysis for special types of data, Springer, 2002.

[24] D. Safieddine, A. Kachenoura, L. Albera, G. Birot, A. Karfoul, A. Pasnicu, A. Biraben, F. Wendling, L. Senhadji, I. Merlet, Removal of muscle artifact from eeg data: comparison between stochastic (ica and cca) and deterministic (emd and wavelet-based) approaches, EURASIP Journal on Advances in Signal Processing 2012 (2012) 1–15.

[25] L. Albera, P. Comon, L. Parra, A. Karfoul, A. Kachenoura, L. Senhadji, Ica and biomedical applications, Handbook of Blind Source Separation, Independent Component Analysis and Applications (2009) 793–832.

[26] T. G. Kolda, B. W. Bader, Tensor decompositions and applications, SIAM review 51 (2009) 455–500.

[27] C. Dopierala, P.-Y. Gumérya, M.-R. Frikhaa, J.-J. Thiébaulta, P. Cinquina, F. Bouchera, Digital implantable gastric stethoscope for the detection of early signs of acute cardiac decompensation in patients with chronic heart failure, Actes LAtelier Ia Sante (2019).

[28] M. Šarlija, F. Jurišić, S. Popović, A convolutional neural network based approach to qrs detection, in: Proceedings of the 10th international symposium on image and signal processing and analysis, IEEE, 2017, pp. 121–125.

[29] M. Doyen, D. Ge, A. Beuchée, G. Carrault, A. I. Hernández, Robust, real-time generic detector based on a multi-feature probabilistic method, Plos one 14 (2019) e0223785.

[30] X. Kong, C. Hu, Z. Duan, X. Kong, C. Hu, Z. Duan, Generalized principal component analysis, Principal Component Analysis Networks and Algorithms (2017) 185–233.

[31] Z. Koldovsky, P. Tichavsky, E. Oja, Efficient variant of algorithm fastica for independent component analysis attaining the cramér-rao lower bound, IEEE Transactions on neural networks 17 (2006) 1265–1277.

[32] A. Cichocki, R. Zdunek, A. Phan, S. Amari, Nonnegative matrix and tensor factorizations - applications to exploratory multi-way data analysis and blind source separation, IEEE Signal Processing Magazine 25 (2009) 142–145.

[33] A. P. Wibawa, A. B. P. Utama, H. Elmunsyah, U. Pujianto, F. A. Dwiyanto, L. Hernandez, Time-series analysis with smoothed convolutional neural network, Journal of big Data 9 (2022) 44.

[34] I. E. Livieris, E. Pintelas, P. Pintelas, A cnn–lstm model for gold price time-series forecasting, Neural computing and applications 32 (2020) 17351–17360.

[35] N. V. Rodrigues, L. R. Abramo, N. S. Hirata, The information of attribute uncertainties: what convolutional neural networks can learn about errors in input data, Machine Learning: Science and Technology 4 (2023) 045019.

[36] I. Goodfellow, Y. Bengio, A. Courville, Deep learning, MIT press, 2016.

[37] T. Ulrich, Envelope calculation from the hilbert transform, Los Alamos Nat. Lab., Los Alamos, NM, USA, Tech. Rep (2006).

[38] I. Rezek, S. Roberts, Envelope extraction via complex homomorphic filtering. technical report tr-98-9, Imperial College, London, Tech. Rep (1998).

[39] M. H. Asmare, F. Woldehanna, L. Janssens, B. Vanrumste, Can heart sound denoising be beneficial in phonocardiogram classification tasks*f*, in: 2021 43rd Annual International Conference of the IEEE Engineering in Medicine & Biology Society (EMBC), IEEE, 2021, pp. 354–358.

[40] M. Boulares, R. Alotaibi, A. AlMansour, A. Barnawi, Cardiovascular disease recognition based on heartbeat segmentation and selection process, International Journal of Environmental Research and Public Health 18 (2021) 10952.

[41] V. N. Varghees, K. Ramachandran, Effective heart sound segmentation and murmur classification using empirical wavelet transform and instantaneous phase for electronic stethoscope, IEEE Sensors Journal 17 (2017) 3861–3872.

[42] Y. Zheng, X. Guo, J. Qin, S. Xiao, Computer-assisted diagnosis for chronic heart failure by the analysis of their cardiac reserve and heart sound characteristics, Computer methods and programs in biomedicine 122 (2015) 372–383.

[43] S. Xiao, X. Guo, X. Sun, Z. Xiao, A relative value method for measuring and evaluating cardiac reserve, Biomedical engineering online 1 (2002) 1–5.

[44] J. P. Boehmer, R. Hariharan, F. G. Devecchi, A. L. Smith, G. Molon, A. Capucci, Q. An, V. Averina, C. M. Stolen, P. H. Thakur, et al., A multisensor algorithm predicts heart failure events in patients with implanted devices: results from the multisense study, JACC: Heart Failure 5 (2017) 216–225.

[45] H. S. Norman, J. Oujiri, S. J. Larue, C. B. Chapman, K. B. Margulies, N. K. Sweitzer, Decreased cardiac functional reserve in heart failure with preserved systolic function, Journal of cardiac failure 17 (2011) 301–308.

[46] S. J. Crick, M. N. Sheppard, S. Y. Ho, L. Gebstein, R. H. Anderson, Anatomy of the pig heart: comparisons with normal human cardiac structure, The Journal of Anatomy 193 (1998) 105–119.

[47] P. P. Lelovas, N. G. Kostomitsopoulos, T. T. Xanthos, A comparative anatomic and physiologic overview of the porcine heart, Journal of the American Association for Laboratory Animal Science 53 (2014) 432–438.

[48] G. C. Gabriel, W. Devine, B. K. Redel, K. M. Whitworth, M. Samuel, L. D. Spate, R. F. Cecil, R. S. Prather, Y. Wu, K. D. Wells, et al., Cardiovascular development and congenital heart disease modeling in the pig, Journal of the American Heart Association 10 (2021) e021631.

[49] F. Meissner, M. C. Galbas, S. Szvetics, C. von Zur Mühlen, T. Heidt, A. Maier, M. Bock, M. Czerny, W. Bothe, S. Reiss, Cardioaortic dimensions in german landrace pigs derived from cardiac magnetic resonance imaging, Scientific Reports 14 (2024) 1869.

[50] Y. L. Rusakova, D. S. Grankin, K. S. Podolskaya, I. Y. Zhuravleva, Pigs as models to test cardiovascular devices, Biomedicines 12 (2024) 1245.